NUMERICAL INVESTIGATION OF VORTEX FORMATION AT INTAKE STRUCTURES USING FLOW 3D SOFTWARE

A THESIS SUBMITTED TO
THE GRADUATE SCHOOL OF NATURAL AND APPLIED SCIENCES
OF
MIDDLE EAST TECHNICAL UNIVERSITY

BY

RUÇHAN MÜGE TATAROĞLU

IN PARTIAL FULFILLMENT OF THE REQUIREMENTS
FOR
THE DEGREE OF MASTER OF SCIENCE
IN
CIVIL ENGINEERING

JUNE 2014

Approval of the thesis:

NUMERICAL INVESTIGATION OF VORTEX FORMATION AT INTAKE STRUCTURES USING FLOW 3D SOFTWARE

Submitted by **RUÇHAN MÜGE TATAROĞLU** in partial fulfillment of the requirements for the degree of **Master of Science in Civil Engineering Department, Middle East Technical University** by,

Prof. Dr. Canan ÖZGEN
Dean, Graduate School of **Natural and Applied Sciences** _____

Prof. Dr. Ahmet Cevdet YALÇINER
Head of Department, **Civil Engineering** _____

Assoc. Prof. Dr. Mete KÖKEN
Supervisor, **Civil Engineering Dept., METU** _____

Prof. Dr. Mustafa Göğüş
Co-Supervisor, **Civil Engineering Dept., METU** _____

Examining Committee Members:

Prof. Dr. Burcu ALTAN SAKARYA
Civil Engineering Dept., METU _____

Assoc. Prof. Dr. Mete KÖKEN
Civil Engineering Dept., METU _____

Prof. Dr. Mustafa GÖĞÜŞ
Civil Engineering Dept., METU _____

Assoc. Prof. Dr. Şahnaz Tiğrek
Civil Engineering Dept., METU _____

Özgün Güler, M.Sc.
IOG Engineering _____

Date:
06/06/2014

I hereby declare that all information in this document has been obtained and presented in accordance with academic rules and ethical conduct. I also declare that, as required by these rules and conduct, I have fully cited and referenced all material and results that are not original to this work.

Name, Last Name : Ruçhan Müge Tataroğlu

Signature :

ABSTRACT

NUMERICAL INVESTIGATION OF VORTEX FORMATION AT INTAKE STRUCTURES USING FLOW-3D SOFTWARE

TATAROĞLU, Ruçhan Müge

M.Sc., Department of Civil Engineering

Supervisor: Assoc. Prof. Dr. Mete KÖKEN
Co-Supervisor: Prof. Dr. Mustafa GÖĞÜŞ

June 2014, 50 Pages

Formation of the vortices in a horizontal water intake structure composed of a reservoir-pipe system is investigated using 3D numerical modeling. The geometrical and hydraulic conditions of the system such as pipe diameters, the distance between the side walls of the intake and the flow discharge is altered and the critical submergence depth required for the formation of the vortex for each test is determined. Although it is possible to capture an air-entraining vortex in the numerical model, there is a deviation in the critical submergence depth compared with the experimental results. Scale effect on the formation of air-entraining vortex is also investigated comparing model and prototype simulations.

Keywords: Horizontal intake, Vortices, Vortex formation, Flow-3D

ÖZ

SU ALMA YAPILARINDAKİ VORTEKS OLUŞUMUNUN FLOW-3D YAZILIMI İLE SAYISAL OLARAK İNCELENMESİ

TATAROĞLU, Ruçhan Müge

Yüksek Lisans, İnşaat Mühendisliği Bölümü

Tez Yöneticisi: Doç. Dr. Mete KÖKEN
Ortak Tez Yöneticisi: Prof. Dr. Mustafa GÖĞÜŞ

Haziran 2014, 50 Sayfa

Bir rezervuar-boru sisteminden oluşan yatay bir su alma yapısında vortekslerin oluşumu üç boyutlu sayısal modelleme yöntemi ile incelenmiştir. Boru çapı, su alma yapısı yan duvarları ara mesafesi ve akımın debisi gibi sistemin geometrik ve hidrolik şartları değiştirilmiş ve bu durumların her birisi için yapılacak deneylerde vortekslerin oluşacağı kritik batıklık derinliği tesbit edilmiştir. Sayısal modelde hava çeken vorteks yakalamak mümkün olsa da, deney sonuçlarıyla karşılaştırıldığında kritik batıklık derinliklerinde sapmalar olmuştur. Ölçek etkisinin, hava çeken vortekslerin oluşumu üzerindeki etkisi de, model ve prototip benzeşimlerinin kıyaslanmasıyla araştırılmıştır.

Anahtar Kelimeler: Yatay su alma yapıları, Girdap, Vorteks oluşumu, Flow-3D

To my dear son Ada…

ACKNOWLEDGMENTS

I am grateful to my supervisor Assoc. Prof. Dr. Mete KÖKEN for his outstanding support and patience during my study. He has always encouraged me whenever I underperform.

I would like to thank to my co-supervisor Prof. Dr. Mustafa GÖĞÜŞ for giving me the confidence. As an Istanbul Technical University undergraduate, I feel close to him.

also grateful to all instructors of Hydromechanic Laboratory, especially Prof. smail AYDIN and Prof. Dr. Burcu ALTAN SAKARYA, for their supportive des.

Dr. İ. Kaya ÖZKIN, a precious father of a friend, convinced me for a master degree in a technical field. I would like to express my gratitude to him for his guidance.

Special thanks to Mehmet Ali KÖKPINAR, for never giving up on believing in me. He has always been very motivative during my degree in Middle East Technical University.

I would like to express my appreciation to Özgün GÜLER, IOG Engineering. He provided me consultancy and technical support whenever I needed.

I am very grateful to my friends, who never refused my call for help. Special thanks to Nilay IŞCEN, Ahmet Nazım ŞAHİN, Burhan YILDIZ, Kutay YILMAZ, Ezgi KÖKER, Ali Ersin DİNÇER, Siamak GHARAHJEH and Cüneyt YAVUZ.

I would like to thank to my family members for their support and patience.

This study was supported by TUBITAK (The Scientific and Technological Research Council of Turkey) under Project No: 110M676 which is gratefully acknowledged here.

TABLE OF CONTENTS

LIST OF TABLES

TABLES

LIST OF FIGURES

FIGURES

LIST OF SYMBOLS

b	:	Wall clearance (m)
Di	:	Intake diameter (m)
Fr	:	Intake Froude number
G	:	Gravity acceleration (m/s2)
H	:	The depth of water from bottom to water surface (m)
Lm	:	Model length (m)
Lp	:	Prototype length (m)
Lr	:	Model length scale ratio
Re	:	Intake Reynolds number
Q	:	Intake discharge (m3/s)
Sc	:	Critical submergence measured from the top of the intake pipe (m)
Sc_exp	:	Sc measured in experimental study (m)
Sc_num	:	Sc obtained in numerical study (m)
ωz	:	Vorticity-z (1/s)
z	:	Location of x-y plane on z axis (m)

CHAPTER 1

INTRODUCTION

1.1 Vortex Formation at Intake Structures

The function of an intake is basically to withdraw water safely from the source and divert this water to an intake conduit. The drawn water is mostly used for flood control (spillway), irrigation, electric power generation and water supply. Flow through the intake is a complicated type of flow. The design of an intake is basically consists of the direction, the location and the size of the intake structure. If the intake is close to the water surface to reduce the cost, there occurs the risk of air-entraining vortex formation. If the intake structure is close to the bottom to increase the amount of water available to withdraw, there occurs the risk of sedimentation blockage. Consequently, while designing an intake structure, an optimization must be reached between the cost, safety and efficiency.

Vortex is basically a region of vorticity where flow spins. It has circular motion and leads to circular streamlines. According to Durgin & Hecker (1978), vortices may be formed due to three main categories (Figure 1.1):

a) Eccentric orientation; b) Viscosity induced velocity gradients; c) Eddies formed by obstruction.

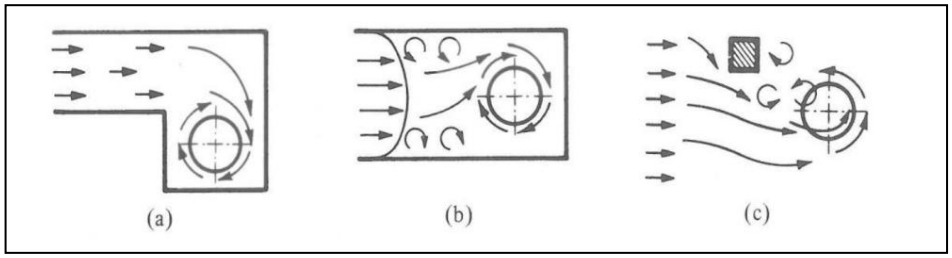

Figure 1.1 Main sources of vortices. Durgin & Hecker (1978)

At intake structures, in the vicinity of the intake, angular velocity increases due to the decrease in cross sectional area. Local drop in pressure, which is a result of spinning motion, causes depression in the water surface. According to the strength of the spinning and the depth of the water, the degree and the shape of the depression can change within a range from a swirl to an air-entraining vortex. Vortex type classifications of Knauss (1987) are shown in Fig. 1.2.

Due to circulation of vortex and its tail, air and debris can be ingested into vortex and carried to intake conduit. It is an undesirable flow condition because it can cause serious operational problems on the hydraulic system.

Submergence depth is the elevation difference between bottom level of the intake and the free surface elevation. It is a crucial concept and related to the sufficiency of depth. Insufficient depth of water above intake could result in the formation of the air-entraining vortices. Critical submergence is the depth just before the vortex formation starts. A dimple is formed if the rotation is small or the submergence is high. The dimple becomes an air core if the rotation gets stronger or the submergence is less.

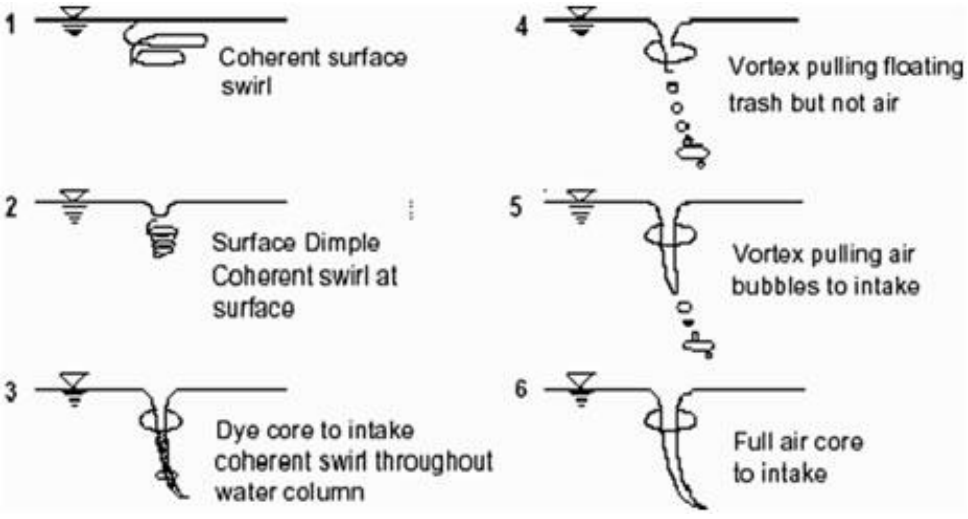

Figure 1.2 Vortex type classifications (Knauss, 1987)

1.2 Vortex Originated Problems

The presence of vortices at intakes may be tolerable to a certain extent. Air-entraining vortices in front of an intake are not tolerable and may cause operational problems such as: result in head losses, generation of vibration and noise on the hydraulic machines, cavitation, reduction in discharging capacity, dam overflowing, decrease in efficiency of pumps, increase in the wearing rate and in the maintenance costs. Using anti vortex devices and increasing the submergence can be counted as basic methods for vortex prevention.

1.3 Scope of the Study

This study is the numerical investigation of the experimental study conducted by Baykara (2013). The aim of that experimental study was to investigate the hydraulic conditions at which air-entraining vortices would form at intake structures.

The present work is aimed to predict the formation of air-entraining vortices at horizontal intakes using a 3D numerical model. Flow-3D software developed by Flow Science Inc. is used to simulate different flow conditions within this study. It is expected that the conclusion of this study will inform the user about the accuracy of the software when it is used as a solver for investigating the hydraulic conditions at which air-entraining vortices occur. This will be done by comparing the experimental results of Baykara (2013) with the numerical results of this present study.

The basic concept of numerical analysis is the digital representation of a flow field. The virtual model that is created with Flow-3D resembles the physical model constructed in the laboratory. After the model is built in the virtual environment, the software enables the user to account for the changes in various flow parameters such as water depth, discharge, wall clearance distance etc. Some of the data among the series of laboratory experiments are processed and the results of simulations for these cases are presented in this study.

An anti-vortex case is simulated to test whether the anti-vortex plates prevent the vortex in the numerical study as it did in the experimental one. In addition to the model scale simulations, prototypes of the two models are simulated to see the scale effect. Moreover, some cases are selected to be resimulated with another viscous solver named Large Eddy Simulation (LES) to see the turbulence effect. These will be explained in detail in Chapter 3 - Numerical Modelling and comparisons will be done in Chapter 4 - Results.

Altough the physical environment is tried to be imitated as good as possible in the numerical model, some constraints such as time limitation and computer capacity limitation are faced during the study. To cope with these constraints, simplifications and assumptions are needed to reduce the complexity of the problem.

CHAPTER 2

LITERATURE REVIEW

Researchers have been carrying out physical model experiments, deriving empirical formulae for a long time to understand the mechanism of the intake vortices. Recently, with the development in the computational power, numerical models are also becoming popular in this field. Researchers have combined theory with measurements to come up with an accurate description of free surface vortex.

In most of the experimental studies, vortices were directly generated by tangential inlet, guide and rotating cylinder. Dye was used for flow visualization. Tracer particles, measuring needles and hot-film anemometer were used to measure the velocity distribution, shape of the free surface and vorticity. A Rankie vortex model was also used to determine the velocity and pressure distributions in the vortex core as an analytical model.

Lugt (1983) provided a non-mathematical introduction to vorticity dynamics. Reddy & Pickford (1972), Odgaard (1986) and Ma et al. (1995) studied the factors influencing the critical submergence. Einstein & Li (1955) and Odgaard (1986) obtained fundamental formulae for tangential velocity and other flow parameters. Hite and Mih (1994) improved and modificated the formulae of surface flow and provided a great advancement. Later, an improvement to Hite's formula by Chen et al (2007) is proposed. Many experimental physical model studies were conducted by Newman (1959), Pritchard (1970), Vatistas et al (1986), Julien (1986) and Mih (1990).

In addition to experimental and empirical investigations, numerical analysis has become a reliable method for engineering problems as a result of advances in computational fluid dynamics (CFD). Today, numerical analysis allows engineers to

create the flow domain, to account changes in the flow parameters, alter the geometry and visualize the results.

Rosenhead (1931) discretized the infinite line of vorticity sheet into a finite number of discrete point vortices. The numerical calculations were done for 2, 4, 8 and 12 elemental vortices. The results were told to be of the same nature but it is believed that the increase in the number of elemental vortices accelerates the rolling-up process.

According to Hald and del Prete (1978), the movement of a point vortex was created due to the velocity field induced by the other point vortices and this led to a fake interaction of adjacent vortices. This effect was not mentioned in Rosenhead's study due to the small number of vortices he worked on or limited accuracy of the calculations. Experiments done by Moore (1971) and Takami (1964) revealed that the classical point vortex method was unreliable.

Chorin (1973) presented a numerical method for solving time-dependent Navier Stokes equations at high Reynolds number. The three-dimensional vortex blob method was introduced by Chorin. He smoothed out the velocity field in a circle with center at the point vortex to improve the vortex method. This could be interpreted as replacing the point vortices with blobs of vorticity. The aim of this study was to integrate large frequencies concerned by Chorin's previous studies with a numerical method. This study was considered to be the introduction of modern vortex calculations.

Hald and del Prete (1978) proved the convergence of Chorin's vortex method for the incompressible, two dimensional, inviscid fluid for a short time interval. The flow was governed by Euler's equations. The changes they made led to an improved estimate for the truncation error. Their proof was quite economical because less smoothness was required compared to mathematical theory.

Beale and Majda (1982a) claimed that they constructed a new class of three dimensional, stable, convergent, and economic vortex methods requiring same amount of computational labor as Chorin's algorithms. In paper (a), a 3-D vortex method was formulated and vortex stretching was incorporated through a Lagrangian update. In paper (b), the stability and convergency of the 3-D vortex methods with high order accuracy were proved.

Chorin (1980) used simple line algorithm to determine the location of the front when the flame was advected by the fluid while it was propagating. Chorin (1982) provided a quantitive information about the evolution of a three dimensional vortex and the suitability of the vortex methods for the analysis of turbulence. E.D. Siggia (1985) studied on vortex rings, vortex flaments and shear layers.

Sethian and Salem (1988) described a new graphic environment in which vortex simulations were visualized. The data were generated by the numerical simulations of incompressible, viscous, laminar and turbulent flow over a backward facing step and the graphics were demonstrated. The fluid data might be interactively examined by the researcher by the presence of the display of moving color contours for scalar fields, smoke or dye injection of passive particles and bubble wire tracers for velocity profiles. Input parameters were menu-driven, and images were updated at nine frames per second. A connection machine CM-2 data parallel supercomputer and a CM-2 frame buffer were key components to provide essential real time motion.

Yıldırım and Kocabaş (1995) conducted studies on determination of critical submergence at intake structures. In this experimental study a point sink was superposed with uniform channel flow and the discharge of the sink was kept equal to the discharge of the uniform flow. The critical submergence level was assigned to be equal to the radius of the point sink. Theoretical and empirical studies resulted in a formulation which gave consistent results in the intake in Sakarya River, Turkey.

Rajendran et al. (1998) compared physical model and numerical model of a pump sump. Physical setup formed with complex turbulent flow properties and turbulent flow. Particle image velocimetry and dye were used. Numerical models were based on Reynolds averaged Navier-Stokes equations. In the study, single free surface vortex was predicted successfully but the structure of the formed vortex was somewhat different from the physical case. The size of the vortex was predicted bigger in the numerical model, when compared with the physical one. (Fig. 2.1)

Constantinescu and Patel (1998a) described a numerical model. To validate this numerical model they carried out experiments. Physical model of pump sump setup was formed with complex turbulent flow properties so that free surface and wall attached vortices were allowed and surface tension effects were neglected. The numerical model solved Reynolds averaged Navier-Stokes equations for three dimensional turbulent flow in a water-pump vertical intake bay with the two-layer k-ε turbulence model.

Locations, size and strength of vortices were compared using the coarse, medium and fine mesh. It was estimated that 2 million points will be needed to substantially reduce the grid dependence. The comparison results indicated that in general, the numerical simulations predicted the number and location of the vortices but the predicted values of maximum vorticity were lower than those measured. Circulation strengths for the vortices were also found different, except for the vortex attached to the side wall nearer to the intake pipe. The study proposed that meandering structure of the vortices in a pump sump created difficulty for numerical problems to simulate vortices properly. However, the validation of the study (Rajendran et al 1999) suggested that the numerical model was a useful engineering tool and could be employed in preliminary design to identify geometric configurations and flow parameters that might lead to strong vortices in the intake and swirl in the suction column.

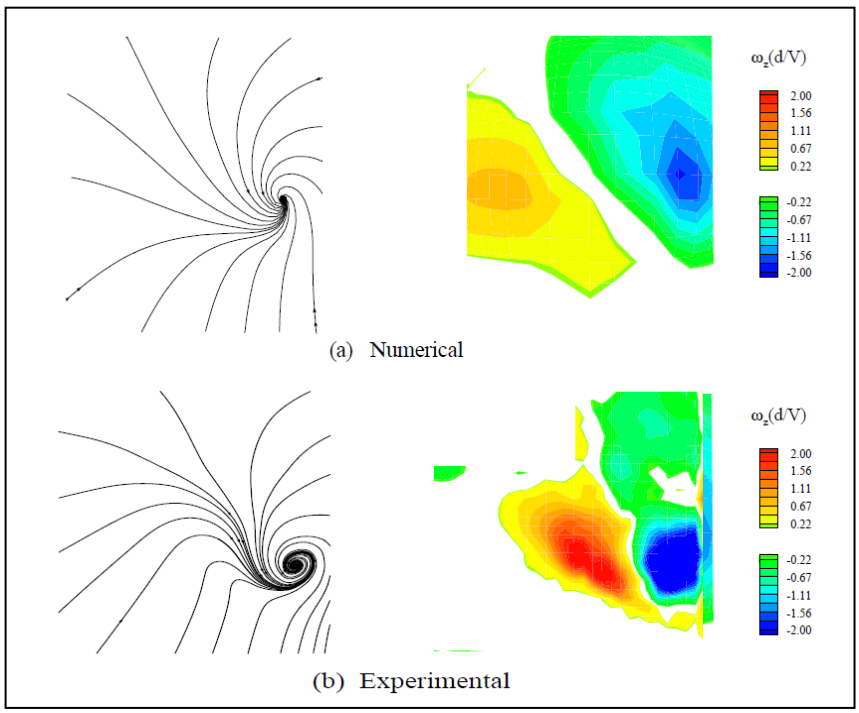

Figure 2.1 Comparison of numerical and experimental results in terms of streamlines and vorticity (Rajendran et al. 1998)

Nagahara et al. (2003) investigated the flow structure of the vortex in a pump suction intake to evaluate the accuracy of CDF calculation. Vortices were generated by experimental apparatus and velocity fields around vortices were measured by particle tracking velocimetry (PTV). It was observed that the maximum velocities obtained instantly were larger than the time averaged ones and radii of the cores were smaller due to the unsteady movement of the vortex. The paper suggested that the steady-state CFD calculation cannot predict the velocity profile around the vortex center accurately although the mesh was fine enough. Two cases are selected randomly in Figure 2.2 to show the difference between measured and calculated profiles mentioned in the paper. (Fig. 2.2)

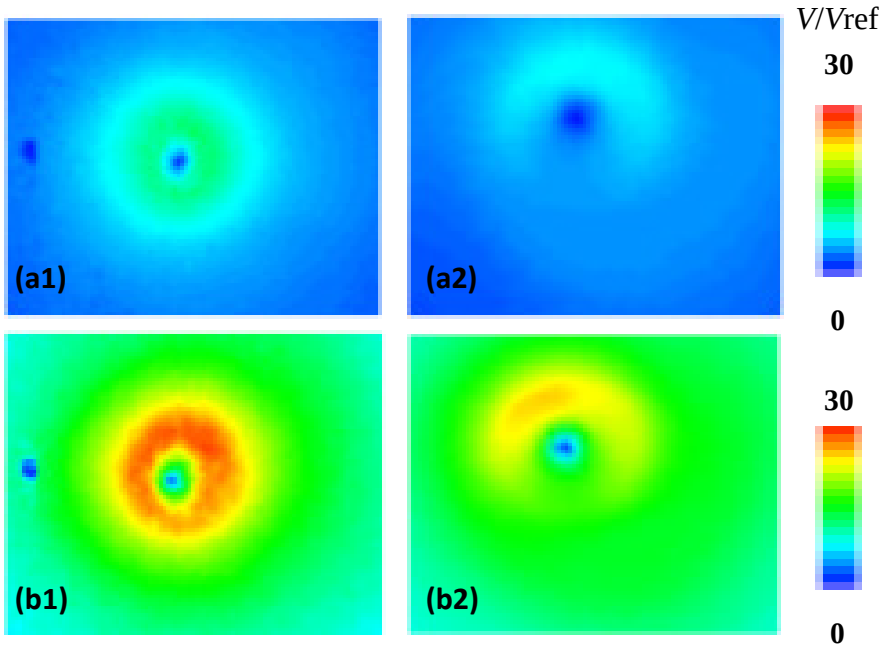

Figure 2.2 Velocity magnitude contour of the measurement and CFD results (Nagahara et al, 2003) a1) case 1 measured; a2) case 1 calculated; b1) case 2 measured; b2) case 2 calculated

Yıldırım (2004) investigated the critical submergence in a rectangular intake. In the study, the setup was superposing of line sink and uniform flow. Experiments were conducted on a horizontal intake pipe sited in a dead-end canal flow. The study gave reasonable results when distances between the dead end solid wall and the intake do not get much smaller than the critical submergence. Otherwise the results would have been overestimating the actual ones by 80 %. (Fig. 2.3)

Okamura et al. (2007) conducted numerical studies on pump sumps in numerical basis with several CFD programs, to compare with physical model. It was noted that, at physical model, required critical submergence levels were increasing nearly proportional with the flow rate in the sump. It was also stated that vortex formations were in the forms of air core and unsteady. Velocity and vorticity distributions were obtained by using particle image velocimetry. According to the findings, when an air-entraining vortex was formed due to the high velocities and low submergence

level, a subsurface vortex was accompanying. In the numerical area, some CFD codes proved to be successful to give outputs with adequately accurate values for industrial usage. However, distribution of magnitudes of vorticity was different from the physical case, may be caused from the lack of accuracy of the CFD computation.

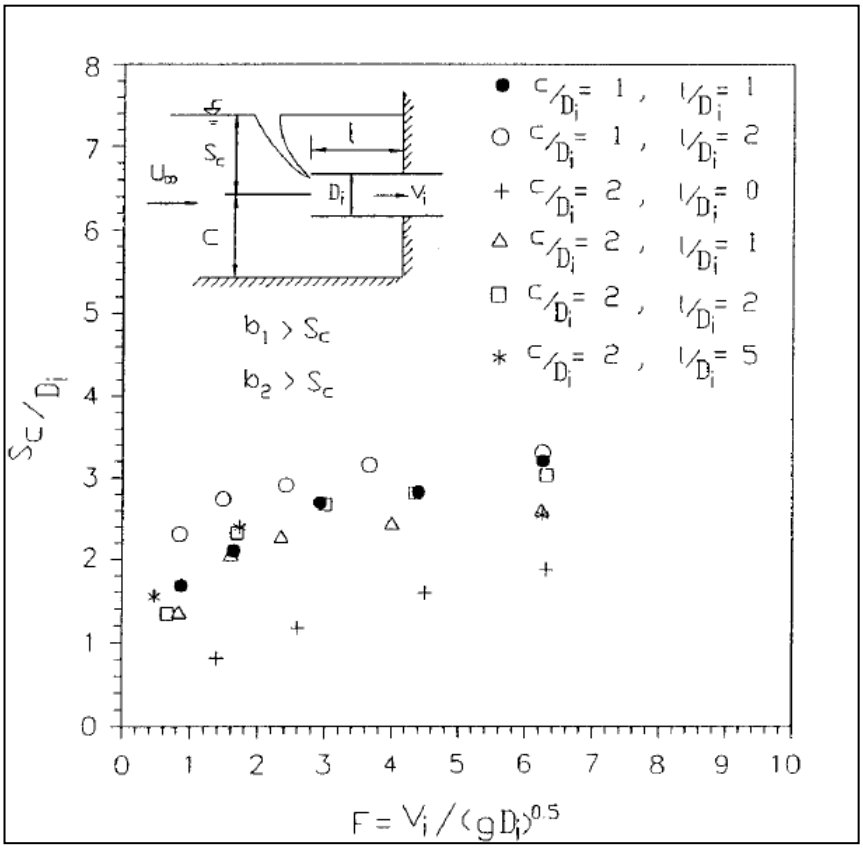

Figure 2.3 Variation of Critical Submergence with Intake Froude Number
(Horizontal Intake Pipe Passing through Vertical Dead End Wall)
(Yıldırım et al. 2004)

Li et al(2008) compared the experimental data and numerical results and got a satisfactory result. Experimental equipments were set up to investigate the formation and evolution of the free surface vortex. The study suggested that the numerical simulation agrees with the practical flow field outside of the vortex core due to the acute changes in the core. The tangential velocity distribution was found to be similar to observations but the radial velocity was slightly different in the vortex

functional region. The vortex core was determined at different depths. The position and structure of the air core predicted by the numerical model was consistent with the physical model.

CHAPTER 3

NUMERICAL MODELLING

3.1 General Description

Flow-3D is a powerful computational fluid dynamics (CFD) code, based on solving the Navier Stokes Equations. Flow-3D uses finite volume approximations of the mass, momentum and energy equations in three dimensions to analyze the complex fluid problems. It also has models for sediment transport, moving rigid bodies, flows in porous media, etc.

Civil engineering flow problems often involve free-surfaces. Free-surface is handled with various ways in many computer programs. Flow-3D uses Volume of Fluid (VOF) technique which was first reported by Hirt et al. (1975) and by Hirt and Nichols (1981). VOF is a powerful free surface tracking method for sharp interfaces. Gas and liquid generally move independently but the interface forms a thin viscous boundary layer. Instead of computing the flow in both gas and liquid regions, VOF defines the air by a boundary condition and applies it on the surface. It is not an independent flow solving algorithm.

There are five main tabs the user will go from one to another while designing the applicable model. These tabs are:

1- Navigator: This is the screen that user will see the simulation files, portfolio summary and the path of the location of the simulation files.

2- Model Setup: The flow domain is designed, the meshing is done, the physical and the numerical parameters are entered. There are six sub tabs at model setup tab.

2.1- General: The finish time of the simulation, compressibility of the fluid, type of interface, type of the units, number of fluids and the degree of precision are determined at this sub tab.

2.2- Physics: There are many physics related options depending on the case such as air entrainment, gravity, fluid source, sediment, cavitation, heat transfer, viscosity and turbulence, moving objects.

2.3- Fluids: The working fluid and its properties are chosen at this sub tab.

2.4- Meshing & Geometry: The geometry of the domain is created, initial and the boundary conditions are entered at this tab. The user can either use the software's drawing options or import an executable drawing file with STL extension. Flow-3D allows user to create a primitive mesh that fits to geometry.

2.5- Output: The desired intervals and types of data are determined here. Restart data interval defines how often the data will be saved in case of a need for restart. Selected data interval defines the size of the steps of timeline while analyzing the solutions. In this study, the restart data is entered as 0.1 sec. and the selected data is entered as 0.01 sec for models and 0.5 sec for prototypes. The information entered at this tab effects the size of output files.

2.6- Numerics: This sub tab contains options about stability factors, convergence controls, viscous stress and pressure solver options, momentum advection and fluid flow solver options.

3- Simulation: This screen provides information about the progress of the simulation. Graphics related to the simulations such as time step size, pressure iteration count etc. can be examined here when needed.

4- Analyze: This tab enables the user basically to analyze the results as a text or in 1D, 2D and 3D plots. Iso surface and color variables are chosen among the options

according to the object of the study. Any time interval and any part of the system can be chosen to analyze. This will save time.

5- Display: This is the screen where user will see the visual results based on the criteria chosen at the analyze tab. Taking a snapshot of the screen or making a movie is possible.

3.2 Model Setup

The geometry of the hydraulic system is created by the drawing module of the software. Four solid components are created in rectangular prism shapes. One of them represents the bottom of the canal. Two of them represent two walls in the system, including one horizontal and one vertical. These impervious walls exist to prevent the fluctuations while water is entering the system. The last one is created to form the intake pipe. One cylinder is created and the component type is set to "hole". When this hole component in cylinder shape is added to the rectangular prism in the downstream, a pipe is obtained. This is done to prevent any problem that may occur if the thickness of the pipe is smaller than the grid size. No surface roughness for any solid component is defined so they are considered as smooth by the solver. Figure 3.1 shows the basic design of the model used in this study.

Simulations' finish times are set to 50 seconds for models and 100 seconds for prototypes. Other parameters are set as follows; interface tracking is free surface, flow mode is incompressible, number of fluids is one, unit is SI units. Double precision is selected among the version options to have a higher precision.
Fluid source model is activated to create a solid component that provides water to the system. Mass source represents the inflow pipe used in the physical model. The change of the discharge of the mass source is entered in a table. Discharge is gradually increased in order not to cause a wave formation in the reservoir. Gravity is defined acting on the negative z direction as -9. 81 m/s^2. Viscous solver is set to laminar for most of the cases and LES (Large Eddy Simulation) for some cases.

Water at 293 K is chosen as the working fluid. Momentum and continuity equations are selected to be solved among the fluid flow solver options.

Initial condition is basically the state of the system when the time is zero. For this study the only initial condition is the fluid elevation. This is one of the parameters that will be changed frequently while vortex formation is being investigated.

Direction of flow where the water enters the system from the mass source and leaves it through the intake pipe is taken as +X direction. Left side of the flow direction is taken as +Y direction. Center of the intake pipe is located at Y=0 m. Wall clearance range is from –b to +b. Direction of depth from bottom to the surface is taken as +Z. The elevation of the bottom of the intake pipe and the base of the canal is taken as Z=0 m. Water depth in the reservoir is h. The values of h and b change from case to case.

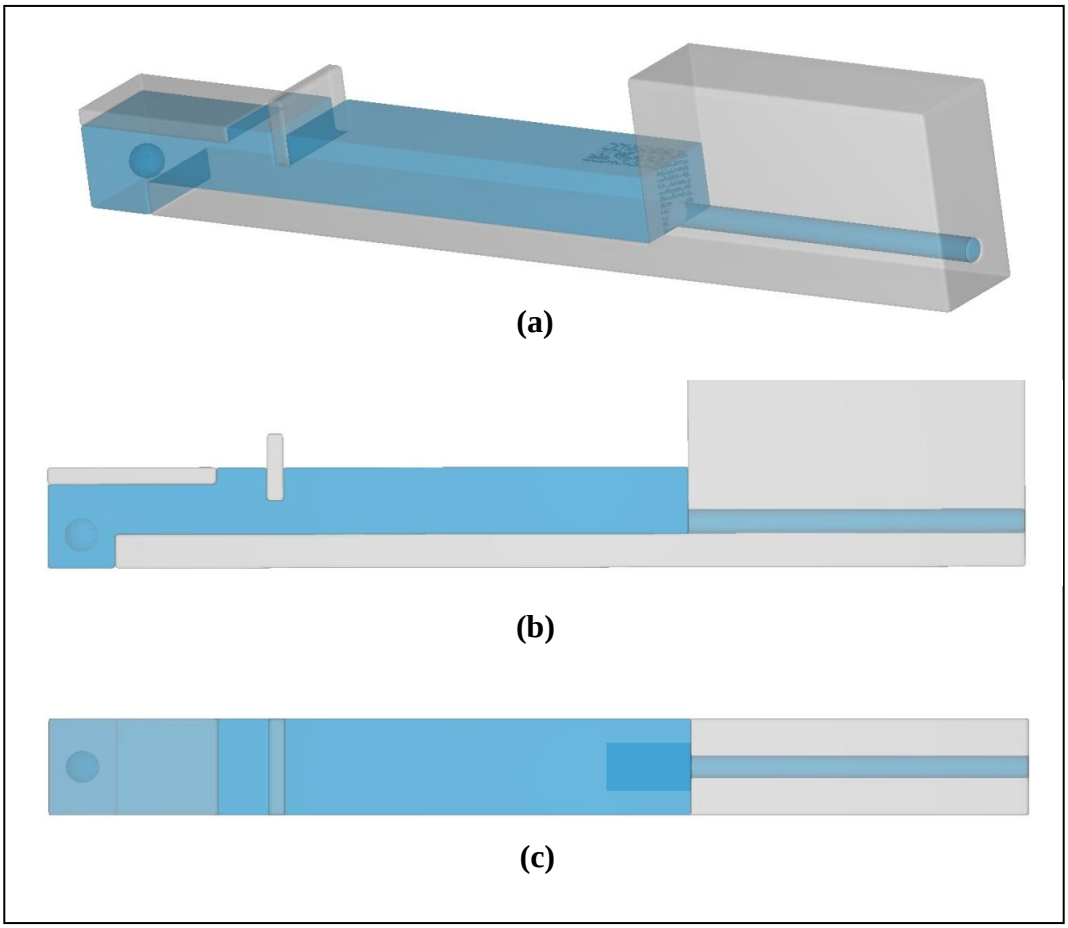

Figure 3.1 Basic Numerical Model: a) perspective view b) side view c) top view

3.3 Grid Generation and Boundary Conditions

FLOW-3D grid generation technique uses structured, rectangular and Cartesian mesh that is independent from the geometry used so that offers the user the simplicity and flexibility. After the geometry is built, a proper computational domain size must be decided before starting the grid generation. It must be large enough to prevent any impose caused by upstream and downstream boundaries. On the other hand, oversized domain will cause an increase in computational time. The length of the domain is selected as 1.80 m in this study whereas width is taken as variable. A mesh block that fits to the geometry is created to start the grid generation. Regardless of

the type of the viscous solver, the grid size is preferred to be kept in the logarithmic region.

Grid size is taken as 0.015 m and simulation is done with one mesh block. Vortex is not observed and it is estimated that failure is most probably due to the inadequate grid size. Considering the fact that refining the whole mesh will increase the solution time, another mesh block with half size is created at a small region close to the intake where air-entraining vortex is expected to appear. Grid size of the inner mesh block is taken as 0.0075 m. This inner mesh provides a denser local resolution without increasing the number of total grid cells much.

It is necessary to denote here that one mesh block is used for the prototype simulations instead of two mesh blocks. The mesh size is kept same with the model's mesh size, but since the geometry is enlarged by the length ratio, total mesh increases as well. The final check of the grid size is made by a grid dependency test by obtaining numerical solutions using different grid resolutions. Grid dependency will be explained in detail in section 3.5.

The Fractional Area-Volume Obstacle Representation (FAVOR) is a technique that enables the program to fractionally divide parts to solid region and fluid region. Favor option is an aid to test if the mesh size enables the solver perceives the whole geometry of the system accurately.

After grid generation and using FAVOR algorithm to finalize the design of the model accurately, boundary conditions have to be set. Figure 3.2 shows the numerical model with mesh planes and boundary conditions. Each face of a mesh block must represent a boundary condition. In this study, there are no side walls defined as solid components but the boundary conditions on the side faces of outer mesh block are determined as wall (W). Wall means solver treats "W" faces as solid components with no slip condition. Top and bottom faces of the outer mesh are determined as symmetry (S). Symmetry means no flow across the "S" plane and velocity normal to symmetry line is zero. Upstream face of the outer mesh block is set to wall. The

inflow is provided by a mass source instead of an inflow pipe as in the laboratory experiment. Downstream face of the outer mesh is set to a volume flow rate (Q). The solver will keep the discharge on “Q” face at the defined rate. Value of volume flow rate is given in a table because it increases gradually up to a point and gets constant after that. This table is kept exactly the same as the mass source table in order to keep the water volume constant within the tank, like in a reservoir. Six faces of the inner mesh block are set to grid overlay (G). This boundary condition is used when a nested mesh is defined in the domain.

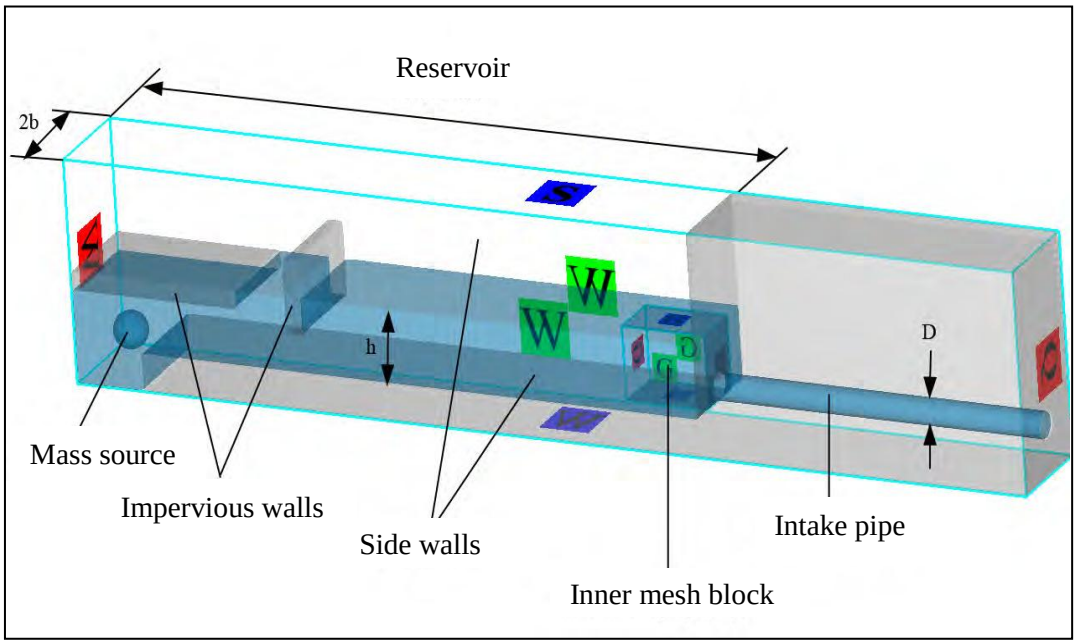

Figure 3.2 Final Numerical Model

After different models and mesh designs are tested to get the most accurate template for the model, the fundamental design of the model is fixed. The numerical model is ready to run different simulations with modified scenarios. Different scenarios are created by changing the parameters such as pipe diameter, water level, discharge and side wall clearance. At each simulation initially a water body is put inside the pipe and the reservoir up to the required depth.

3.4 Viscous Solver

Flow is selected to be viscous and no-slip option is chosen as a wall shear condition. Momentum advection affects both run time and accuracy. Since swirling flow conditions are present within the flow, momentum solver is selected to be second order. Renormalized group model (RNG) is selected among viscous solver options. First simulation is done with RNG model but it did not yield reasonable results. The reason is thought to be the intermittency of the vortex and the dissipative nature of the RANS model. Altough the flow is actually turbulent the velocities at vortex region are comparatively low. Therefore the flow is assumed to be laminar to prevent the dissipative effect of Reynolds Averaged Navier-Stokes (RANS) models. After all cases are simulated as laminar, two cases are selected to be simulated with LES turbulence model to see the effect of turbulence. The comparison is done in the conclusion part.

3.5 Grid Dependence

Grid size is very critical in numerical solutions. Inadequate grid resolution will result in inaccuracy. An initial grid size is attained in the previous section. Before starting the numerical investigation, the grid dependency check must be done. This check is basically running the simulation of a specific case with different mesh sizes by refining the mesh at each step. The grid independency will be approved when the results of the last two simulations are close to each other. If two different grid sizes are used for the same model and if both give almost the same results, then it is wiser to use the coarser grid size because the finer one takes longer simulation time and ends up with larger output files.

One of the cases of the experimental study is selected as a model. The numerical model is built for this case. The proper grid size is attained and simulations are run until the air- entraining vortex is seen. The mesh dependency check for this study is done by running a simulation for this model with a finer mesh. The 3D images and

the out of plane vorticity contours close to the free surface are presented in Figure 3.3 and 3.4. The information about the mesh and the geometry of the selected model is given in Table 3.1.

Table 3.1 Model and Mesh Information

D=0.144 m b=0.3 m h=0.397 m	Coarser mesh	Finer mesh
Total number of mesh blocks	2	2
Mesh block 1	910.960	1210.880
Mesh block 2	142.040	192.104
Total number of cells	1.053.000	1.402.984
Vortex appearance time (sec)	23.50	22.2 and 39.3

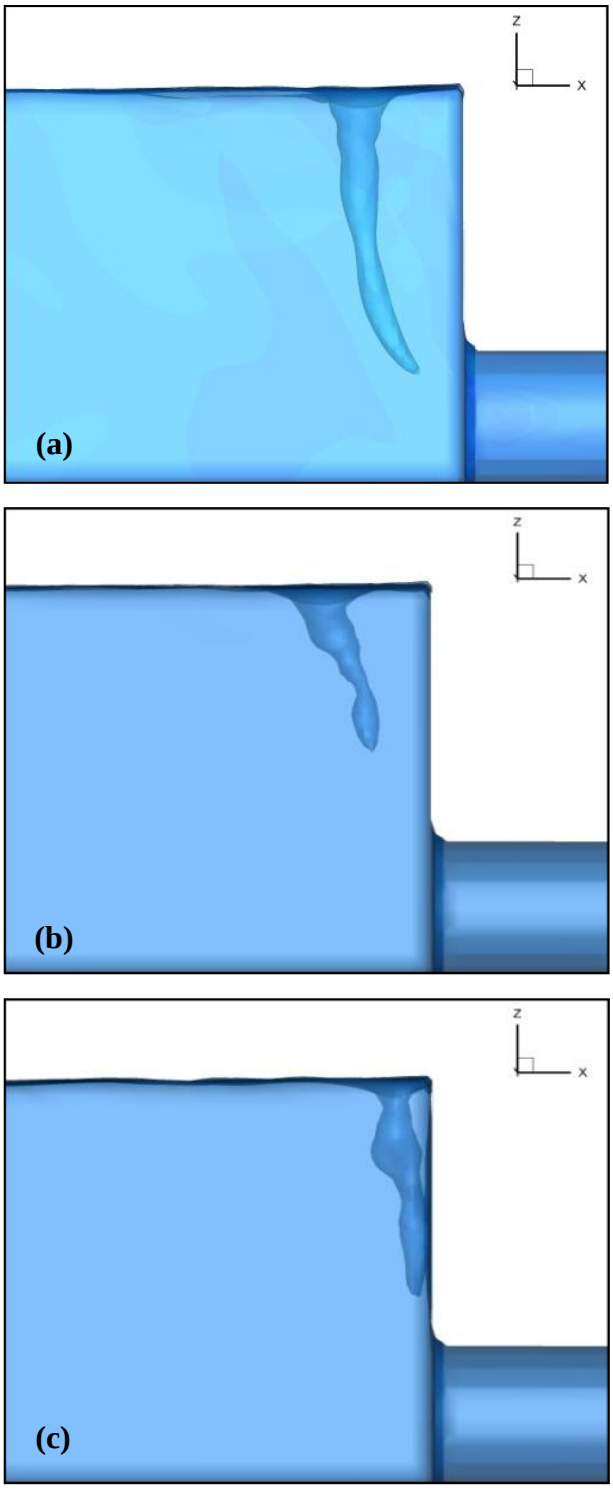

Figure 3.3 Comparisons of 3D Images for Grid Dependency:
a) Coarse mesh; b) Fine mesh vortex at 22.2 sec; c) Fine mesh vortex at 39.3 sec.

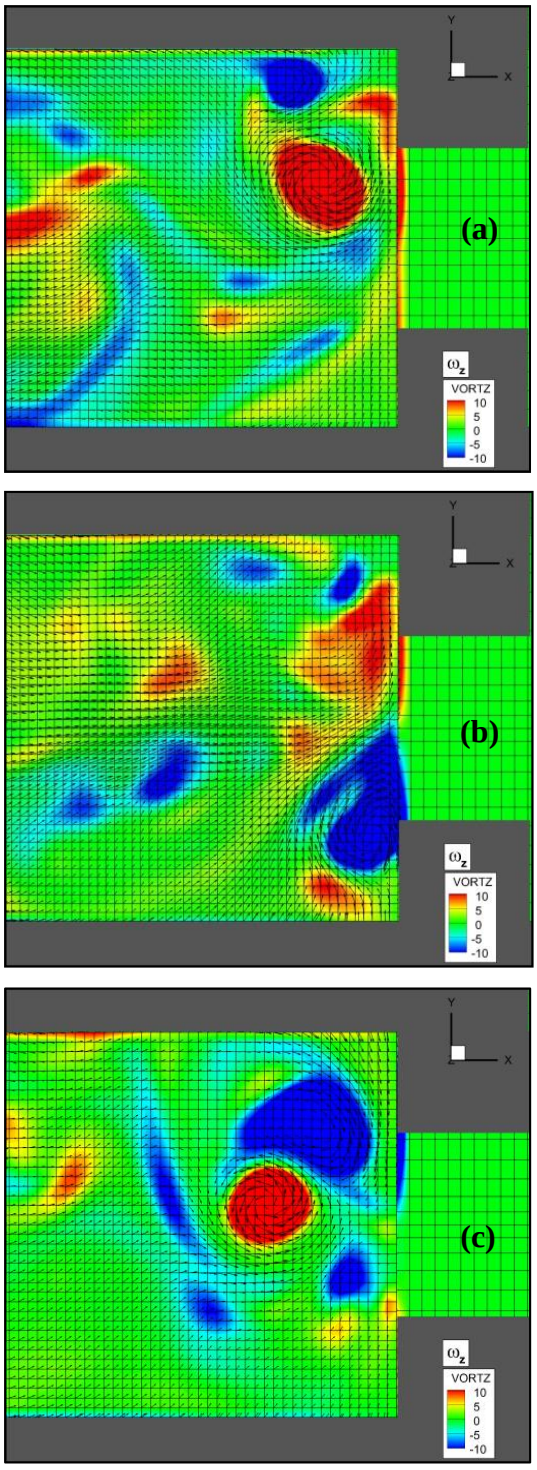

Figure 3.4 Comparisons of Vorticity Contours for Grid Dependency [ω_z (1/sec)]: a) coarse mesh out of plane vorticity contour of vortex on a horizontal plane close to free surface; b) Fine mesh out of plane vorticity contour of 1st vortex on a horizontal plane close to free surface; c) Fine mesh out of plane vorticity contour of 2nd vortex on a horizontal plane close to free surface.

Air-entraining vortex is obviously seen in both mesh sizes where the strength of the vortices are comparable. Coarser mesh ended up with a very acceptable result so there is no need to further refine mesh and increase the difficulty that already exists due to the time and computer constraints.

In this study, the number of grid points for the models varies from 400.000 to 1.000.000, and the number of grids for the prototypes varies from 3.500.000 to 4.000.000 depending on the sidewall clearance b and flow depth h. Figure 3.5 shows the grid of the model case that has 1.053.000 grid points including outer and inner mesh blocks.

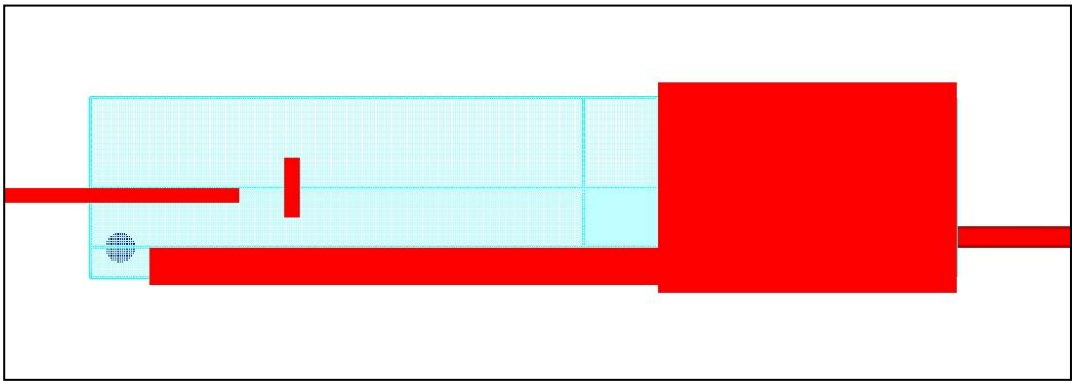

Figure 3.5 Mesh Grids and Solid Components

CHAPTER 4

RESULTS

4.1 Outline of the Simulations

The outline of the simulations is given in Table 4.1. The table contains information about the cases simulated, type of viscous solver used for the corresponding case, geometry of the model, water level at which vortex is seen and the critical submergence of numerical and experimental studies.

In fact there are much more simulations conducted within this study as the water depth is initially selected to be large and decreased with increments of 0.5 m for models and 1.0 m for prototypes until the air-entraining vortex is captured. Therefore the cases presented in Table 4.1 are only the last simulations at each case where air-entraining vortex was observed.

It is obviously noticed that the critical submergence values obtained with numerical solution are quiet lower than the experimental ones. When LES model is used instead of laminar solution, it yields more accurate submergence values. This improvement is related to resolution of turbulence close to the walls in the LES model which was not possible in the laminar solution. Although LES is able to decrease the error to some extent; there still exists a noticeable gap between numerical and experimental results. To investigate the possible reasons of this inconsistency, vortex formations are interpreted through different comparisons.

Table 4.1 Outline of the Simulations

Case No	Case Description	Viscous Solver	b (m)	D (m)	Q (m3/sec)	h_num (m)	Sc Numerical (m)	h_exp (m)	Sc Experiment (m)
1	D=0,100 m								
a	Model	Laminar	0.20	0.100	0.0517	0.315	0.215	0.765	0.665
b	Model	Laminar	0.30	0.100	0.0517	0.268	0.168	0.368	0.268
c	Model	Laminar	0.50	0.100	0.0517	0.237	0.137	0.487	0.387
d	Prototype of 1-b	Laminar	6.00	2.000	92.3970	6.360	4.360	N/A	N/A
e	Model 1-a	LES	0.20	0.100	0.0517	0.315	0.215	0.765	0.665
f	Model 1-a	LES	0.20	0.100	0.0517	0.515	0.415	0.765	0.665
2	D=0,144 m								
a	Model	Laminar	0.20	0.144	0.0626	0.350	0.206	0.899	0.755
b	Model	Laminar	0.30	0.144	0.0626	0.397	0.253	0.397	0.253
c	Model	Laminar	0.50	0.144	0.0626	0.350	0.206	0.496	0.352
d	Prototype of 2-b	Laminar	6.00	2.880	111.8962	7.940	5.060	N/A	N/A
e	Prototype of 2-b	Laminar	6.00	2.880	111.8962	8.940	6.060	N/A	N/A
f	Model 2-b w/antivortex plate	Laminar	0.30	0.144	0.0626	0.397	0.253	N/A	N/A
g	Mesh dependency test on 2-b	Laminar	0.30	0.144	0.0626	0.397	0.253	0.397	0.253
3	D=0,194 m								
a	Model	Laminar	0.20	0.194	0.0626	0.340	0.146	0.839	0.645
b	Model	Laminar	0.30	0.194	0.0626	0.340	0.146	0.440	0.246
c	Model	Laminar	0.50	0.194	0.0626	0.380	0.186	0.530	0.336
d	Model 3-b	LES	0.20	0.194	0.0626	0.340	0.146	0.839	0.645

4.2 Effect of Sidewall Clearance

Three different wall clearance (b) values are considered at a fixed pipe diameter (D). Fixed diameter is selected as D= 0.144 m. The numerical and experimental submergence values (Sc_num and Sc_exp) and the corresponding wall clearances are organized in Table 4.2 to examine the change in the accuracy of numerical solution under sidewall effect. There is not a direct relationship between the sidewall clearance, b, and accuracy of the numerical results. The numerical and experimental solutions are in perfect agreement for b = 0.3 m, whereas the numerical results underestimates the submergence depth by 72% and 41% for sidewall clearance values of 0.2 m and 0.5 m respectively. Smallest sidewall clearance gives the highest error in these set of simulations. Air-entraining vortices are visualized for the three cases investigated in Figure 4.1 by plotting the air-water interface. In Figure 4.1, one can see that vortex cores are getting smaller and smaller as they go deeper inside the water. Hence, it is not possible to visualize the full air-entraining vortex, which is supposed to enter into the intake pipe, as this requires a very fine grid resolution. Out of plane vorticity contours together with the velocity vectors are shown on a horizontal plane that cuts through a plane close to the free surface for the three sidewall clearance values in Figure 4.2. One can see that the out of plane vorticity contours are amplified inside the core of air-entraining vortices. However there are some other patches of high vorticity other than the ones generated by the air-entraining vortices. Vortex strengths in all the three cases investigated are comparable. The vortex observed in the smallest sidewall clearance is not as clear as the others (Fig. 4.1a). It appears on the corner of the outer mesh (Fig. 4.2a). In the experimental study conducted by Baykara, it is mentioned that only for b = 0.2 m cases, the vortices occur at the boundaries near the plexiglass side-walls which agrees with the numerical finding here. At wall clearance of 0.3 m, a clear air-core vortex is seen in front of the intake, along the pipe center (Fig. 4.2b). At wall clearance of 0.5 m, the air-entraining vortex is diverted from the pipe center (Fig. 4.2c).

Table 4.2 Effect of Sidewall Clearance

D=0.144 m	b=0.2 m	b=0.3 m	b=0.5 m
Sc_num (m)	0.206	0.253	0.206
Sc_exp (m)	0.755	0.253	0.352
Error (%)	-72.1	0.0	-41.4

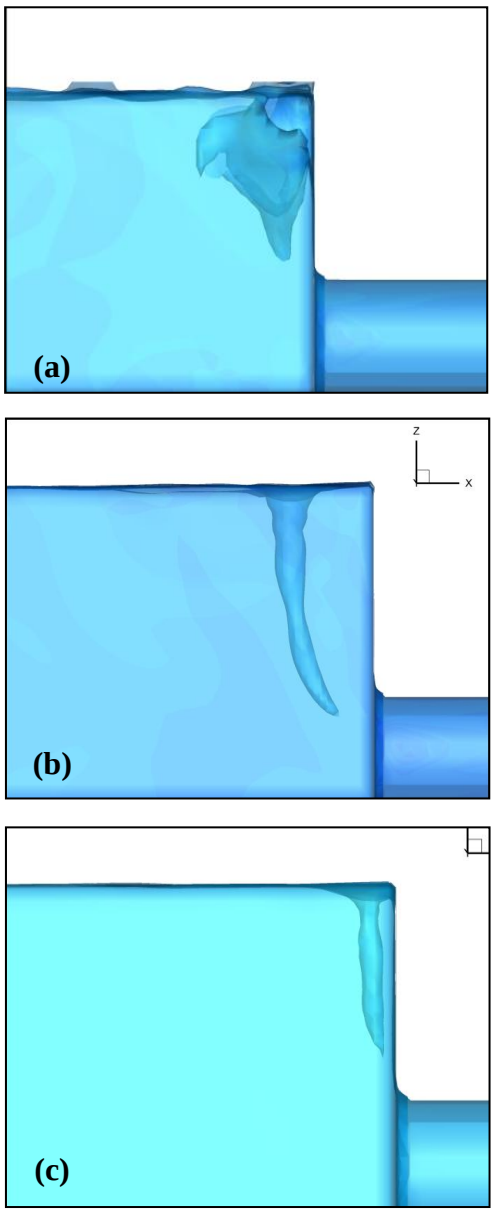

Figure 4.1 Visualization of the air-entraining vortex by plotting air water interface at wall clearance lengths of: a) b=0.2 m; b) b=0.3 m; c) b=0.5 m.

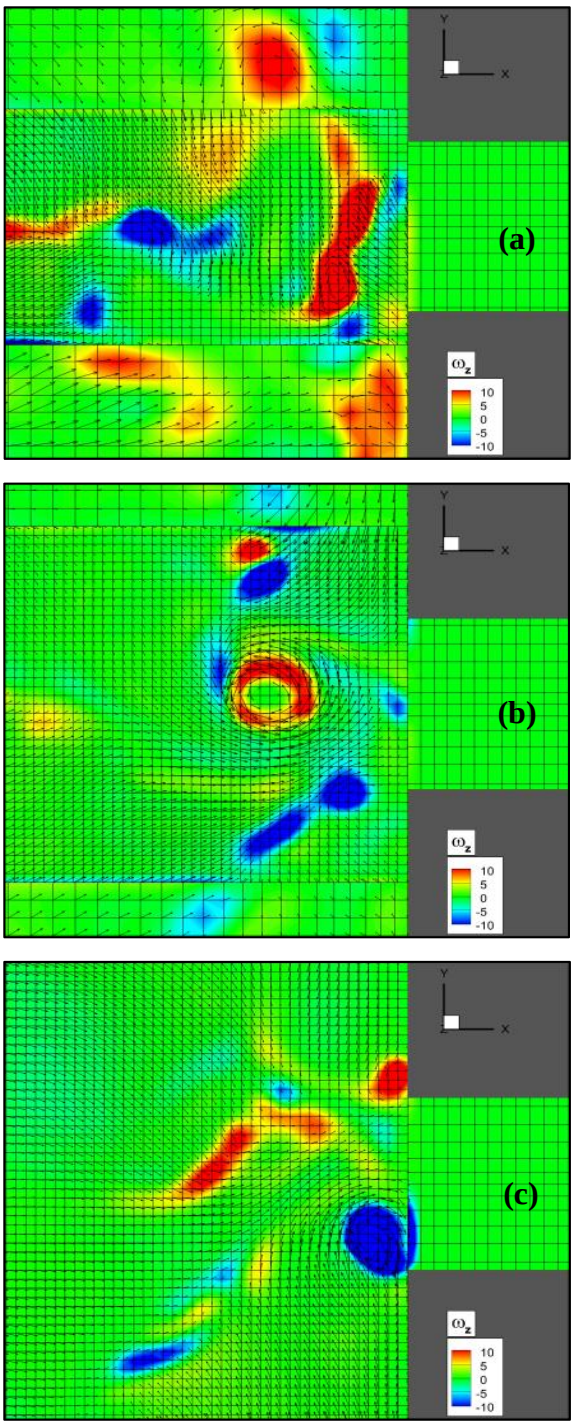

Figure 4.2 Velocity vectors and out of plane vorticity contours, ω_z (1/sec), on a horizontal plane cutting through a plane close to the free surface at wall clearance lengths of: a) b=0.2 m; b) b=0.3 m; c) b=0.5 m.

4.3 Effect of Pipe Diameter

Three different pipe diameters (D) are considered at a fixed wall clearance (b). Fixed clearance is selected as b=0.3 m. The numerical and experimental submergence values (Sc_num and Sc_exp) and the corresponding pipe diameters are organized in Table 4.3 to examine the change in the accuracy of the numerical solutions at different pipe diameters. Air-entraining vortices are visualized for the three cases investigated in Figure 4.3 by plotting the air-water interface. Moreover, out of plane vorticity contours together with the velocity vectors are shown on a horizontal plane that cuts through a plane close to the free surface for the three sidewall clearance values in Figure 4.4. There is no direct relationship between the pipe diameter D and the accuracy of the numerical results. The numerical solutions underestimate the critical submergence depth by 37.31% and 40.65% for pipe diameters of 0.100 m and 0.194 m respectively. Compared to the other two pipe diameters, air-entraining vortex is smaller in size for the largest pipe diameter of 0.194 m (Fig. 4.3c). In this case, vortex forms at a slightly asymmetrical position with respect to the intake pipe axis whereas it is almost at a symmetrical position in the other two cases (Fig. 4.4c).

Table 4.3 Effect of Pipe Diameter

b=0.3 m	D=0.100 m	D=0.144 m	D=0.194 m
Sc (m)	0.168	0.253	0.146
Sc_exp (m)	0.268	0.253	0.246
Error (%)	-37.31	0.0	-40.65

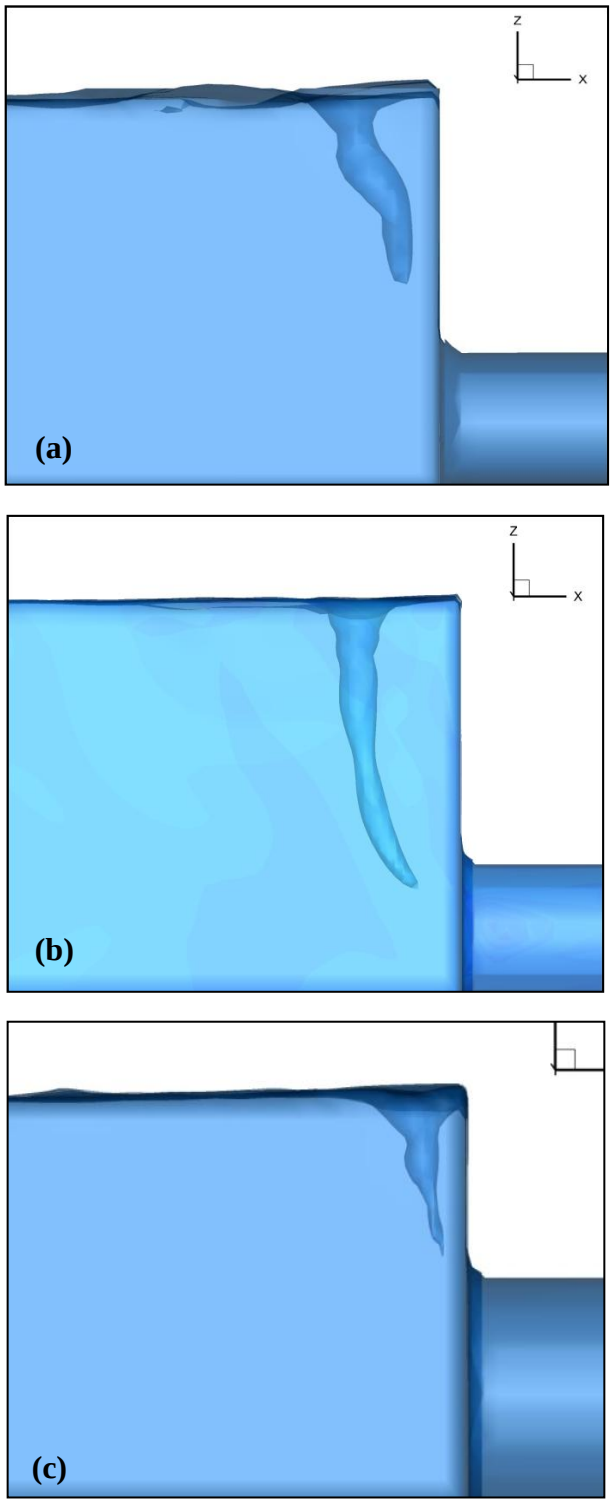

Figure 4.3 Visualization of the air-entraining vortex by plotting air water interface at pipe diameter lengths of: a) D=0.100 m; b) D=0.144 m; c) D=0.194 m.

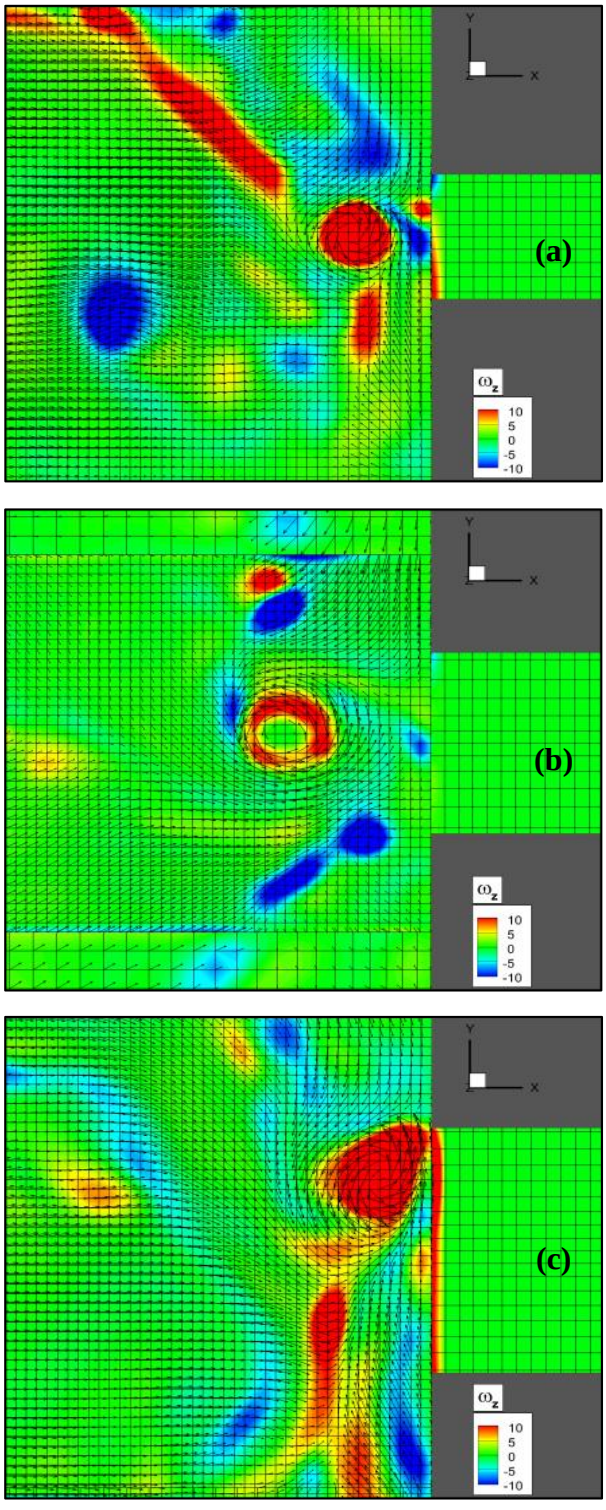

Figure 4.4 Velocity vectors and out of plane vorticity contours, ω_z (1/sec), on a horizontal plane cutting through a plane close to the free surface at pipe diameter lengths of: a) D=0.100 m; b) D=0.144 m; c) D=0.194 m.

4.4 Effect of Anti-vortex Plate

The anti-vortex devices used in the experimental study are 10 rectangular plexiglass plates in different lengths and widths. In this study initially a 50 mm x10 mm plate is selected among the plates those gave satisfactory results. It is placed in the numerical model of Case 2b on the top of the intake, tangent to the pipe entrance. Although this plate scaled down the original vortex at the end of the simulation, the result is not found satisfactory. It is then replaced with a 50 mm x 20 mm plate. This time, the results of the simulation were quite satisfactory in terms of preventing the air-entraining vortex. The effect of the anti-vortex plate can be seen in Figures 4.5 and 4.6. Three dimensional images obviously demonstrate that the air-entraining vortex close to the intake turns into a short and weak vortex far from the intake after anti-vortex plate is placed.

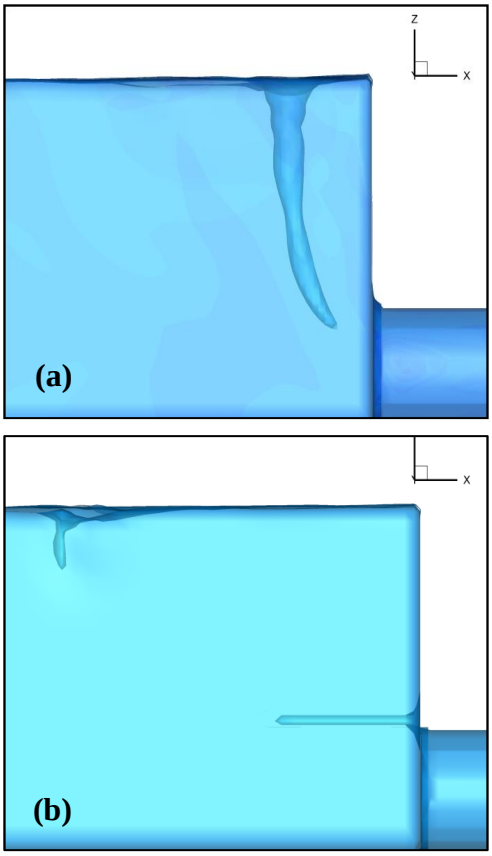

Figure 4.5 Visualization of the vortex by plotting air water interface (D=0.144 m. b=0.3 m) in cases of: a) without anti-vortex plate; b) with anti-vortex plate.

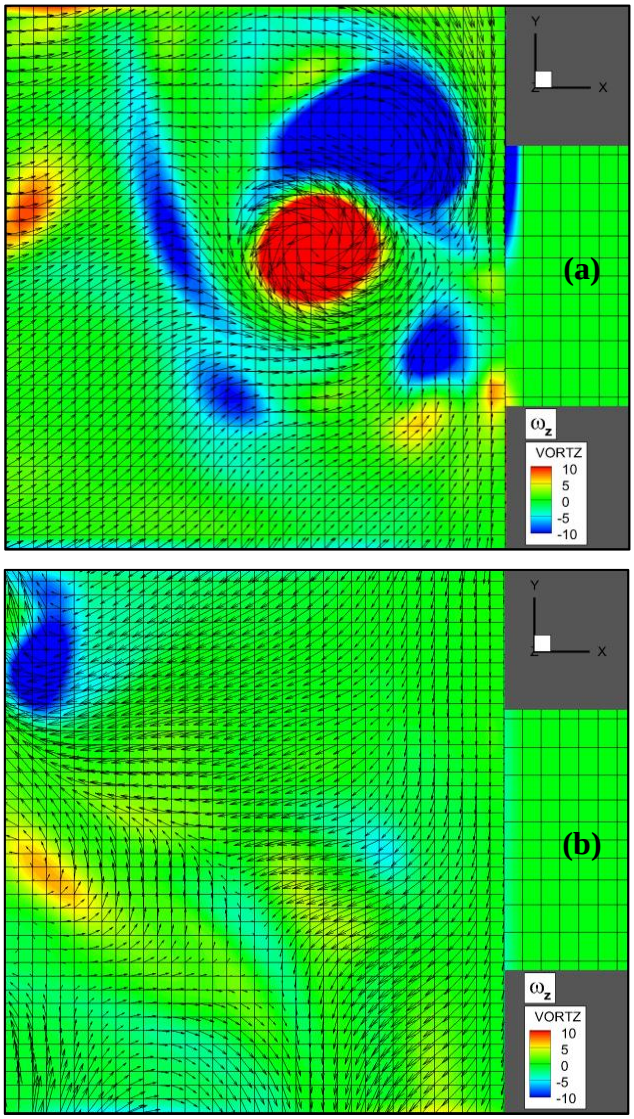

Figure 4.6 Velocity vectors and out of plane vorticity contours, ω_z (1/sec), on a horizontal plane cutting through z=0.38 m (D=0.144 m. b=0.3 m) in cases of: a) without anti-vortex plate; b) with anti-vortex plate.

4.5 Model Scale Effect

To evaluate the scale effect by using Flow3D, prototypes of Case 1d and 2b are built by enlarging the model geometry by length ratio (Lr). Lr is assumed to be 1/20 in this study. The discharges of the prototypes are calculated by equating the Froude numbers of model and prototype. The submergence depth for the prototype is calculated by multiplying the submergence depth of the model by 20. The critical submergence of the prototype is expected to be higher than the corresponding value obtained by multiplying the critical submergence depth of the model by 20 because of the scale effect. Therefore, the prototype simulations are repeated by increasing the critical submergence by 1.0 m intervals until the vortex is not seen. In the prototype simulations air-entraining vortex was present up to the flow depth of 8.94 m. As expected the air-entraining vortex was observed at a higher elevation than the one observed in the model scale. Figure 4.7 and 4.8 are prepared to visualize the vortex seen in Case 2b and Case 2d. Vortex is visualized at a flow depth of h = 0. 397 m in the model scale and at h = 8.94 m in the prototype scale. One important difference between the model scale and the prototype scale is that it is not very easy to identify a clear air-water interface in the prototype scale (Fig. 4.7b). As the size of the air-entraining vortex increases in the prototype scale it is possible to visualize the tail of the air-entraining vortex entering into the intake pipe. A lower horizontal plane is cut to see the vorticity contour of the prototype more clearly (Fig. 4.8)

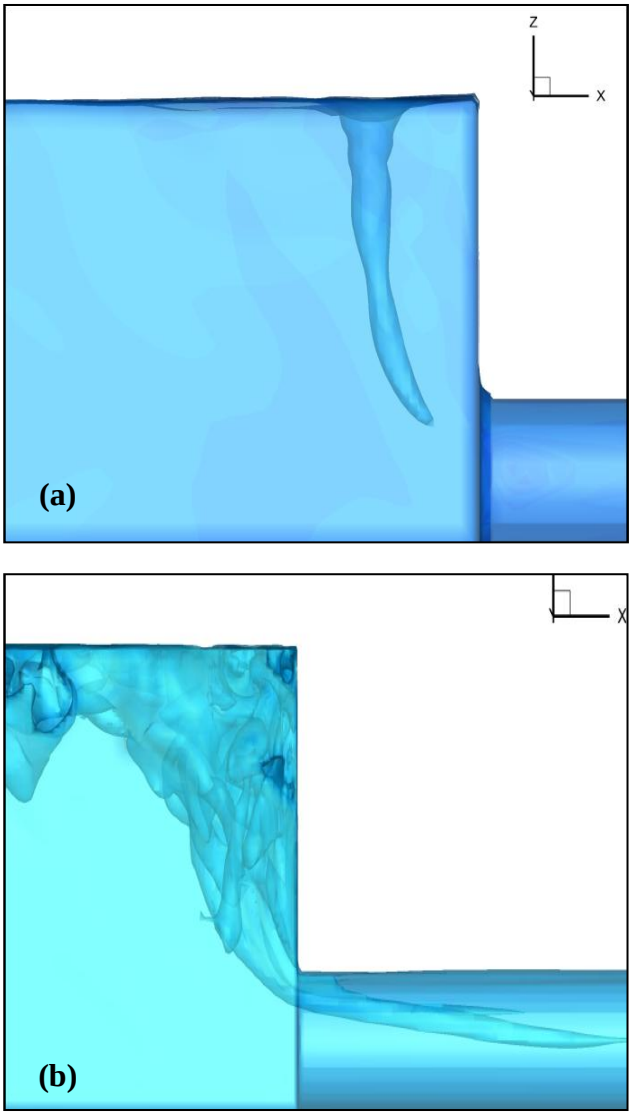

Figure 4.7 Visualization of the air-entraining vortex by plotting air water interface for: a) Case 2b at model scale (h=0.397 m); b) Case 2d at prototype scale (h=8.94 m).

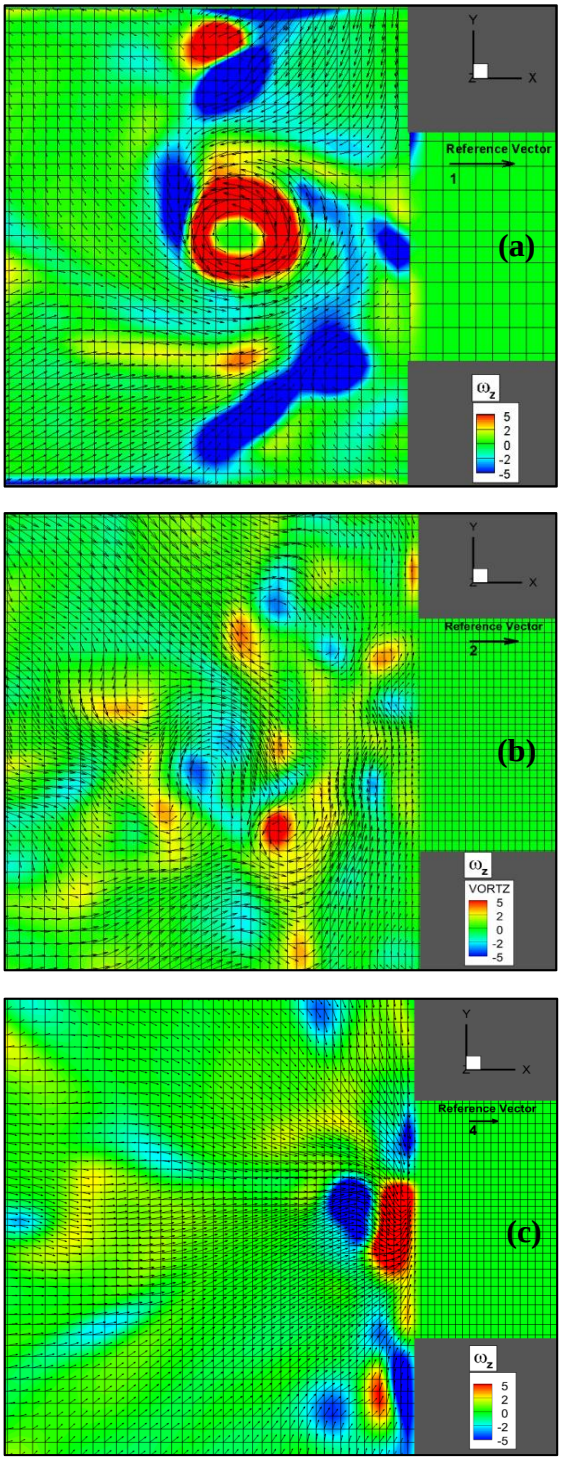

Figure 4.8 Velocity vectors and out of plane vorticity contours, ω_z (1/sec) for : a) on a horizontal plane close to the free surface Case 2b at model scale (h=0.397 m); b) on a horizontal plane close to the free surface Case 2d at prototype scale (h=8.94 m); c) on a horizontal plane at z=3.5 m Case 2d at prototype scale (h=8.94 m).

4.6 Effect of Turbulence Model

Cases with the narrowest wall clearance are selected to be resimulated with LES turbulence model to better capture the turbulence close to the sidewalls and to eliminate any kind of error arising from modelling this part wrong. Table 4.4 summarizes the critical submergence depths obtained for two cases those are simulated with both Laminar and LES solvers. It is obvious that higher submergence values are obtained with LES which are closer to the experimental results. Air-entraining vortices are visualized for laminar and LES solution in Figure 4.9 by plotting the air-water interface. Moreover, out of plane vorticity contours together with the velocity vectors are shown on a horizontal plane at z=0.3 m for the laminar and LES solutions in Figure 4.10. In the LES model, air-entraining vortex is forming close to the sidewall whereas in the laminar solution it forms close to the centerline of the intake pipe. In fact this difference is evidence that LES is better in capturing the flow near the sidewalls compared to the laminar model. If the air-entraining vortex is originated from the vorticity generated close to the sidewalls than LES model does a better job in capturing it.

Table 4.4 Effect of Turbulence Model

b=0.2 m	Laminar	LES	Sc_exp (m)
Sc_num (m) D=0.100 m	0.215	0.415	0.665
Sc_num (m) D=0.194 m	0.146	0.246	0.645

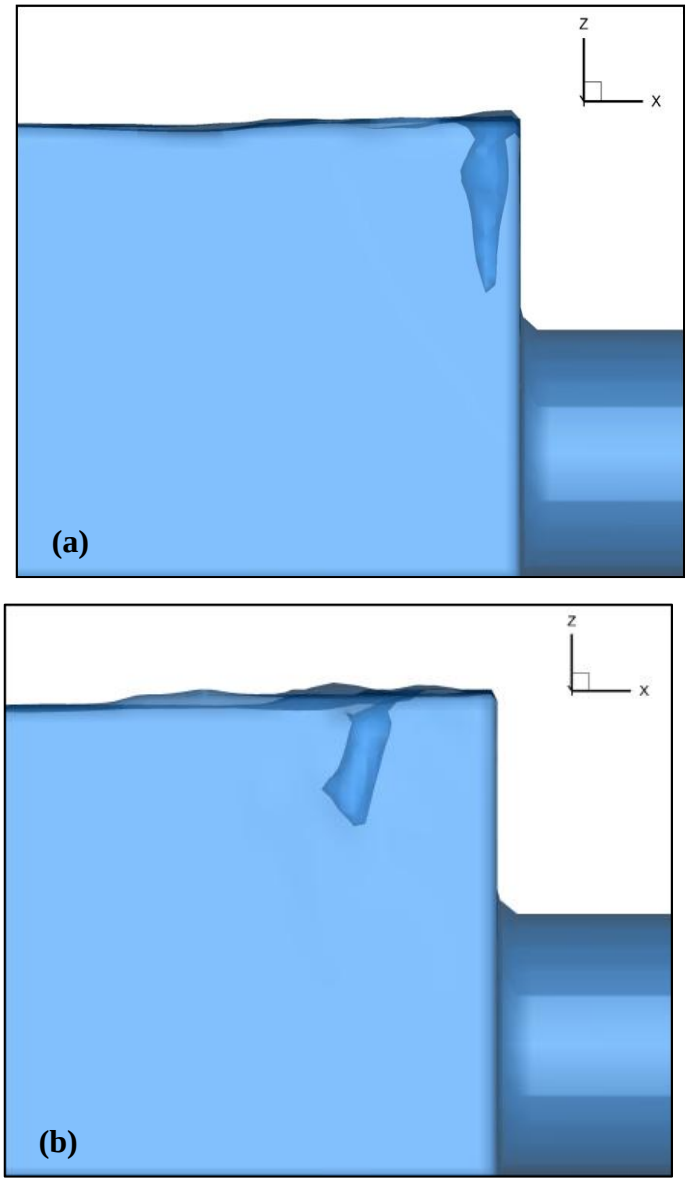

Figure 4.9 Visualization of the air-entraining vortex by plotting air water interface with the solver types of: a) laminar; b) LES

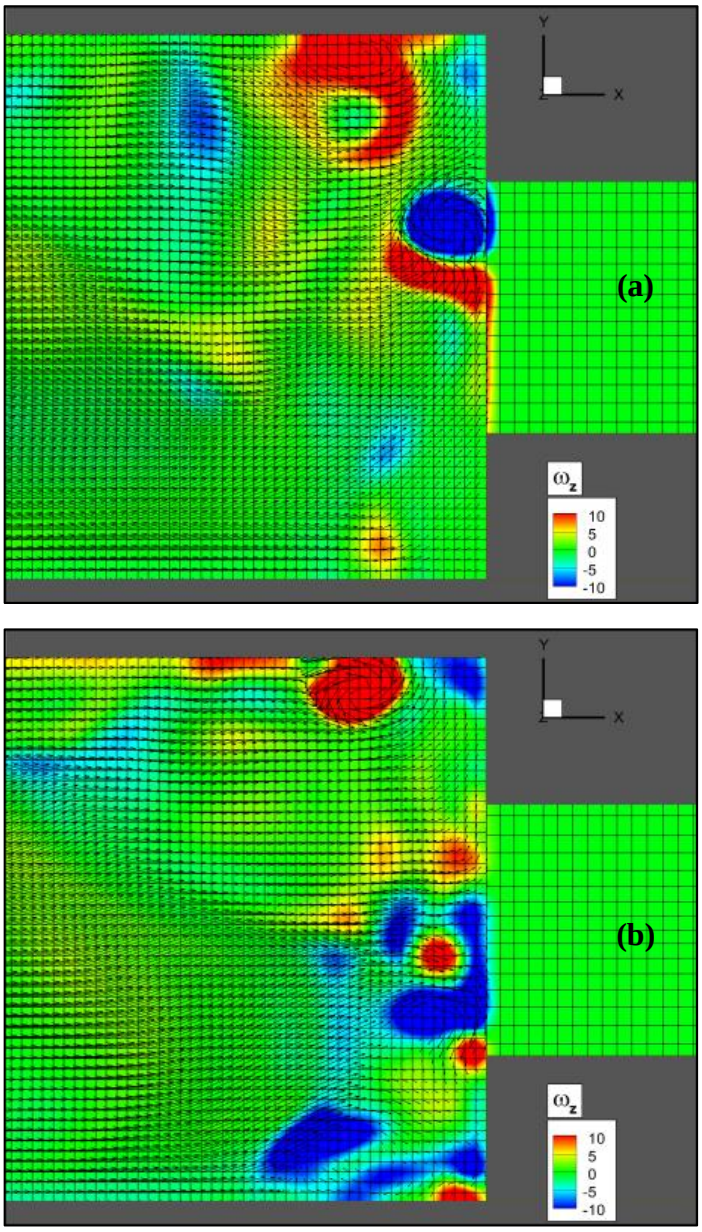

Figure 4.10 Velocity vectors and out of plane vorticity contours, ω_z (1/sec), on a horizontal plane at z=0.3 m with the solver types of: a) laminar; b) LES

4.7 Comparison of Experimental and Numerical Results

As mentioned before in this chapter, the fluid heights in which air-entraining vortex is captured by Flow3D are different from the ones obtained from the physical experiments. Table 4.5 gives us an idea about how much the critical submergence values are lower than the ones obtained from the experiments in each case. The viscous solver for most of the simulations presented in this table is laminar but LES turbulence model is used for some cases to observe the effect of viscous solver on the accuracy of the solution.

Table 4.5 Comparison of Experimental and Numerical Results

Case no	Case Description	h (m)	Sc_{num} (m)	Sc_{exp} (m)	$[(Sc-Sc_{exp})/Sc_{exp}]*100$ %
	D=0.100 m				
1a	model b=0.2	0.315	0.215	0.665	-67.67
1b	model b=0.3	0.268	0.168	0.268	-37.31
1c	model b=0.5	0.237	0.137	0.387	-64.60
1f	model b=0.2 w/LES	0.515	0.415	0.665	-37.59
	D=0.144 m				
2a	model b=0.2	0.350	0.206	0.755	-72.71
2b	model b=0.3	0.397	0.253	0.253	0
2c	model b=0.5	0.350	0.206	0.352	-41.47
	D=0.194 m				
3a	model b=0.2	0.340	0.146	0.645	-77.36
3b	model b=0.3	0.340	0.146	0.246	-40.60
3c	model b=0.5	0.380	0.186	0.336	-44.64
3e	model b=0.2 w/LES	0.440	0.246	0.645	-61.86

According to Table 4.5 the error in laminar solution of Case 1a is 67. 67 % and it drops to 37.59 % when LES is used. This obviously means that transforming the viscous solver from laminar to LES resulted in reduction in the error. For Case 3e, the error dropped from 77.36 % to 61.68.

While large errors exist and they are decreased to some extent by LES solver, Case 2b resulted in a perfect agreement with laminar solver. This behavior is tried to be

explained with the relationship between 2b/Di and Sc/Di given by Baykara (2013). Baykara (2013), stated that according to the non-dimensional sidewall clearance, 2b/Di, the non-dimensional critical submergence depth Sc/Di is observed at different flow depths for a given pipe diameter. These results are classified as maximum, minimum or intermediate non-dimensional critical submergence depths, Sc/Di. Threshold values for 2b/Di are given for different pipe diameters in Table 4.6.

According to the study, the maximum values of Sc/Di are measured at the smallest 2b/Di values of an intake pipe and the minimum Sc/Di values are measured at following larger 2b/Di values. Table 4.7 shows the variation of errors in the simulations conducted within this study according to the Sc/Di classification presented by Baykara (2013). It is noticed that the error is the highest for maximum Sc/Di values, minimum for the minimum Sc/Di values, and in between these two for intermediate Sc/Di values. Table 4.8 is prepared to show the errors in ascending order. This table shows that error increases as the Sc/Di changes from minimum to maximum.

Table 4.6 2b/Di Values of the Intake Pipes of Di Resulted in Maximum, Minimum and Intermediate Sc/Di (Baykara, 2013)

Di (cm) / 2b (cm)	10	14.4	19.4
40	4.00	2.78	2.06
60	6.00	4.17	3.09
100	10.00	6.94	5.16
2b/Di values result in intermediate Sc/Di			
2b/Di values result in minimum Sc/Di			
2b/Di values result in maximum Sc/Di			

Table 4.7 2b/Di Categorization of Errors in terms of Maximum, Minimum and Intermediate Sc/Di

Case No	2b/Di	Error (%)	Sc/Di Type
1a	4.00	-67.67	Maximum
1b	6.00	-37.31	Minimum
1c	10.00	-64.60	Intermediate
1f (1a with LES)	4.00	-37.59	Maximum
2a	2.78	-72.72	Maximum
2b	4.17	0.00	Minimum
2c	6.94	-41.48	Intermediate
3a	2.06	-77.36	Maximum
3b	3.09	-40.65	Minimum
3c	5.16	-44.64	Intermediate
3e (3a with LES)	2.06	-61.86	Maximum

Table 4.8 Ascending Order of Errors of Laminar Solutions with Corresponding Sc/Di Type and Pipe Diameter

Case no	Error (%)	Sc/Di Type	Di (cm)
2 b	0.00	Minimum	14.40
1 b	-37.31	Minimum	10.00
3 b	-40.65	Minimum	19.40
2 c	-41.48	Intermediate	14.40
3 c	-44.64	Intermediate	19.40
1 c	-64.60	Intermediate	10.00
1 a	-67.67	Maximum	10.00
2 a	-72.72	Maximum	14.40
3 a	-77.36	Maximum	19.40

CHAPTER 5

CONCLUSION

In this study, the numerical model of a physical experiment is built by Flow-3D. Simulations for different cases are run to investigate the hydraulic conditions at which air-entraining vortices appear. The critical submergence values are obtained and compared with the experimental results. To enrich the numerical investigation the effects of wall clearance and pipe diameter are evaluated, the effect of change in viscous solver is tested and prototypes for some cases are simulated to see the scale effect. A model with a horizontal anti-vortex device is also built and simulated. The conclusions of this numerical study can be listed as the following:

1) The extents of the errors depend directly on the relation between the values of 2b/Di and Sc/Di as defined in Baykara (2013). 2b/Di values that result in minimum Sc/Di values give the minimum error. 2b/Di values that result in maximum Sc/Di values give the maximum error. 2b/Di values that result in intermediate Sc/Di values gives the intermediate error.

2) Altough an exact result is obtained in one case with laminar solution, there are many results those are incompatible with the experimental study. Critical submergence values obtained by this numerical study are lower than the critical submergence values obtained by experimental study.

3) It can be suggested that LES model gives better solutions for small 2b/Di values. Because laminar solver is not able to capture the vorticity near the walls that is resulting from the turbulence once 2b/Di values are small which is affecting the formation of air-entraining vortex.

5) Acceptable results are obtained for the case with anti-vortex plate. The vortex is prevented successfully in the numerical model as it is prevented in the experiment.

6) The observation time in the experimental study was approximately 5 minutes. In this study simulations are run for 50 seconds for models and 100 seconds for the prototypes. Therefore simulation time is quiet short when compared to the experimental study in order to cope with the time and capacity constraints. Not having a chance to run the simulations longer, the solver might have missed the opportunity of capturing the vortices at higher submergence depths.

7) Flow-3D is convenient software to use for capturing air-entraining vortices at intakes. Altering the parameters and observing their impacts are easier when compared to experimental studies.

As a future study, conditions at which air-entraining vortices appear can be investigated for asymmetric cases.

REFERENCES

Aydın, İ. (2001), *"CE 580 Computational Techniques for Fluid Dynamics"*, lecture notes, Middle East Technical University.

Aybar, A. (2012), *"Computational Modelling of Free Surface Flow in Intake Structures Using Flow 3D Software"*, thesis submitted to Middle East Technical University.

Baykara, A. (2013), *"Effect of Hydraulic Parameters on the Formation of Vortices at Intake Structures"*, thesis submitted to Middle East Technical University.

Beale J.T., Majda A. (1982a), *"Vortex methods I: Convergence in Three Dimensions"*, Mathematics of Computation, 39, 1-27.

Beale J.T., Majda A. (1982b), *"Vortex methods II: Higher Order Accuracy in Two and Three Dimensions"*, Mathematics of Computation, 39, 29-52.

Chen Y., Wu, C. and Ye, M., Ju, X. (2007), *"Hydraulic Characteristics of Vertical Vortex at Hydraulic Intakes"*, Journal of Hydrodynamics, Ser. B, 19(2): 143-149.

Chorin, A.J. (1973), *"Numerical Study of Slightly Viscous Flow"*, Journal of Fluid Mechanics, 57, 785-796.

Chorin, A.J. (1980), *"Flame Advection and Propogation Algorithms"*, Journal of Computational Physics, 35: 1-11.

Chorin, A.J. (1982), "*The Evolution of a Turbulent Vortex",* Communications in Mathematical Physics, 83, 517-535.

Constantinescu, G., and Patel, V. C. (1998a), *''Numerical Model for Simulation of Pump-Intake Flow and Vortices"*, Journal of Hydraulic Engineering, ASCE. 124(2), 123–134.

Durgin, W.W. and Hecker, G.E. (1978), *"The Modeling of Vortices in Intake Structures"*, Proc IAHR-ASME-ASCE Joint Symposium on Design and Operation of Fluid Machinery, CSU Fort Collins, June 1978 vols I and III.

Einstein, H.A. and Li, H.L. (1955), "*Steady Vortex in a Real Fluid"*, La Houllie Blanche, 483-496.

Flow Science Inc., www.flow3d.com, last visited on April 2014.

Hald O.H. and V.M. del Prete (1978*), "Convergence of Vortex Methods for Euler's Equations"*, Math, Comp., 32, 791-809.

Hirt, C.W., Nichols, B.D. and Romero, N. C. (1975) *"SOLA - A Numerical Solution Algorithm for Transient Fluid Flows,"* Los Alamos Scientific Laboratory report LA-5852.

Hirt, C.W., Nichols, B.D. (1981), *"Volume of fluid (VOF) method for the dynamics of free boundaries",* Journal of Computational Physics, Volume 39, Issue 1: 201–225.

Hite, J.E. and Mih, W.C. (1994), "*Velocity of Air-Core Vortices at Hydraulic Intakes",* Journal of Hydraulic Engineering, ASCE, HY3, 284-297.

Julien, P.Y. (1986), *"Concentration of very Fine Silts in a Steady Vortex"*, J Hydr. Res, 24(4): 255-264

Knauss, J. (1987), *"Swirling Flow Problems at Intakes"*, A.A. Balkema, Rotterdam.

Li, Hai-feng, Chen, Hong-xun, Ma Zheng, et al. (2008), *"Experimental and Numerical Investigation of Free Surface Vortex"*, Journal of Hydrodynamics, 20 (4), 485-491.

Lugt, H.J. (1983), "Vortex *Flow in Nature and Technology"*, Book, 34-35.

Ma, Jing-ming, Huang, Ji-tang and Liu, Tian-xiong (1995), *"The Critical Submergence at Pressure Intakes"*, Water Resources and Hydropower Engineering, 30(5): 55-57.

Mih, W.C. (1990), *"Discussion of Analysis of Fine Particle Concentrations in a Combined Vortex",* Journal of Hydraulic Resources, 28(3): 392-395.

Moore, D.W. (1971), *"The Discrete Vortex Approximation of a Finite Vortex Sheet"*, California Inst. of Tech. Report AFOSR-1804-69.

Nagahara, T., Sato, T., Okamura, T., Iwano, R. (2003), "*Measurement of the Flow Around the Submerged Vortex Cavitation in a Pump Intake by Means of PIV"*, Fifth International Symposium on Cavitation (cav2003) Osaka, Japan, November 1-4.

Newman, B.G. (1959), *"Flow in a Viscous Trailing Vortex"*, Aeronautical Quarterly, X(2): 149-162.

Odgaard, A.J. (1986), "*Free-Surface Air Core Vortex",* Journal of Hydraulic Engineering, ASCE, HY7, 610-620.

Okamura, T., Kyoji, K., Jun, M. (2007), *"CFD Prediction and Model Experiment on Suction Vortices in Pump Sump"*, The 9th Asian International Conference on Fluid Machinery, October 16-19, Jeju, Korea.

Pritchard, W.G. (1970), *"Solitary Waves in Rotating Fluids",* Journal of Fluid Mechanics, 42 (Part 1): 61-83.

Rajendran, V.P., Constantinescu, G.S., Patel V.C. (1998), *"Experiments on Flow in a Model Water-Pump Intake Sump to Validate a Numerical Model"*, Proceedings of FEDSM'98, 1998 ASME Fluids Engineering Division Summer Meeting June 21-25, Washington, DC.

Rajendran, V.P., Constantinescu S.G., and Patel, V.C. (1999), *"Experimental Validation of Numerical Model of Flow in Pump-Intake Bays"*, Journal of Hydraulic Engineering, 125, 1119-1125.

Reddy, Y.R. and Pickford, J.A. (1972), *"Vortices at Intakes in Conventional Sumps"*, Water Power, 108-109.

Rosenhead, L. (1931), "*The Formation of Vortices from a Surface of Discontinuity"*, Proc. Roy. Soc. London Ser. A, 134, 170-192.

Sethian, J.A. and Salem, J.B, (1988), *"Animation of Interactive Fluid Flow Visualization Tools on a Data Paralel Machine"*, Internet. J. Super. Appl., 3.2, 10-39.

Siggia E.D. (1985), *"Collapse and Amplification of a Vortex Filament",* Journal of Physics of Fluids, Vol 28: 794-805.

Takami H. (1964), *"Numerical Experiment with Discrete Vortex Approximation, with Reference to the Rolling Up of a Vortex Sheet"*, Dept. of Aero, and Astr., Stanford University Report SUDAER-202.

Vatistas G.H., Lin S., Kwok C.K. (1986), *"Theoretical and Experimental Studies on Vortex Chamber Flow"*, AIAA J, 24(4): 635-642.

Yıldırım N. and Kocabaş F. (1995*),"Critical Submergence for Intakes at Open Channel Flow"*, Journal of Hydraulic Engineering, ASCE, 121, HY12, 900-905.

Yıldırım, N. (2004), *"Critical Submergence for a Rectangular Intake"*, Journal of Engineering Mechanics, Vol. 130, No. 10, 1195-1210.